SYNOPTIC FEATURES ASSOCIATED WITH TEMPORALLY COHERENT MODES OF VARIABILITY OF THE NORTH PACIFIC JET STREAM

Kyle S. Griffin and Jonathan E. Martin

Department of Atmospheric and Oceanic Sciences, University of Wisconsin-Madison

Corresponding author address: *J. E. Martin,*
1225 W. Dayton Street, Madison WI, 53706
Email: jemarti1@wisc.edu

Submitted to *Journal of Climate*, 20 November 2015
In revised form 16 May 2016
Second revised version: August 16, 2016

Abstract

Time extended EOF (TE-EOF) analysis is employed to examine the synoptic-scale evolution of the two leading modes of the north Pacific jet stream variability, namely its zonal extension/retraction (TE-EOF 1) and the north/south shift of its exit region (TE-EOF 2). Use of the TE-EOF analysis enables a temporally coherent examination of the synoptic-scale evolution preceding and following peaks in each of the two leading modes that provides insight into on the preferred evolutions of the north Pacific jet.

Composite analyses are constructed based upon selecting peaks in the principal component time series of both phases of each TE-EOF whose magnitude exceeded 1.5 standard deviations. Jet extension events are associated with an anomalous cyclonic circulation over the Gulf of Alaska that induces a low-level warm anomaly over western North America. Jet retractions are associated with a nearly opposite configuration characterized by an anomalous anticyclonic circulation over the Aleutians and anomalous low-level cold over western North America. Similar but lower-amplitude upper level patterns are noted in the composites of the corresponding poleward/equatorward shifted jet phases, with the poleward shift of the jet exit region tied to anomalously low geopotential heights over Alaska and anomalous low-level warmth over north central North America. An equatorward shift of the exit region is tied to positive height anomalies over Alaska with downstream cold anomalies occurring in western North America. The more extreme downstream impacts that characterize TE-EOF 2 are also longer lasting (>5 days), suggesting potential utility in medium-range forecasts.

1. Introduction

Among the most ubiquitous structural characteristics of the Earth's atmosphere are the narrow, rapidly flowing currents of air located near the tropopause, known as jet streams or jets. These synoptic features were largely unknown before and during World War II despite their original identification by Wasaburo Ooishi over Japan in 1924 (Lewis 2003). By the end of the war, however, the existence of jet streams was well established, quickly drawing substantial amounts of research attention that quickly led to the discovery of separate subtropical (e.g. Loewe and Radok 1950, Yeh 1950, Koteswaram 1953) and polar (e.g. Namias and Clapp 1944, Palmén 1951, Newton 1954) jets.

The first comprehensive descriptions of North Pacific jet stream structure were provided by Mohri (1953). He emphasized that the jet sat between contrasting air masses and that what often appeared to be a single jet entity was, in fact, a hybrid of the separate subtropical and polar jets. Considerable attention has subsequently been directed toward understanding the influence of external processes on the evolution of the jet. For instance, deep tropical convection, organized on the synoptic-scale, can impact the jet either directly via upper-level divergent outflow (e.g Archambault et al. 2013) or remotely through downstream baroclinic development (e.g. Kiladis and Weickmann 1992, Madden and Julian 1994, Higgins et al. 2000, Riemer and Jones 2010).

To date, the variability of the North Pacific jet and its resultant impacts on the regional and hemispheric flow have been less thoroughly investigated. Schubert

77 and Park (1991) conducted one of the first examinations of the intraseasonal
78 variability of the North Pacific jet by performing an empirical orthogonal function
79 (EOF) analysis on zonal wind filtered for a 20-70 day period. The leading mode of
80 variability described a modulation of the zonal wind intensity in the core of the
81 North Pacific jet, while the second leading mode described a modulation of the zonal
82 extent of the jet. Eichelberger and Hartmann (2007) further highlighted the
83 important role that the modulation of the jet's zonal extent plays in explaining jet
84 variability on weekly time scales over the North Pacific. They attributed one of their
85 analyzed modes of variability to a combination of a north-south shift, pulsing
86 intensity, and extension/retraction of the jet stream over the North Pacific,
87 portraying the variability of the jet on the synoptic scale to be significantly more
88 complicated than that revealed in the analysis of Schubert and Park (1991).
89 Among the earliest study to note the regional impacts of interannual
90 variability of the North Pacific jet was that of Chu et al. (1993). They showed that
91 differences in the zonal extent of the jet had an enormous impact on rainfall in
92 Hawaii as a zonally retracted (extended) jet in 1982-83 (1981-82) was associated
93 with an extremely wet (dry) winter. Otkin and Martin (2004) constructed a synoptic
94 climatology of Kona low frequency near Hawaii using 10 years of ECMWF Tropical
95 Ocean Global Atmosphere (TOGA) surface and upper-air data. They found that a
96 retracted jet was associated with increased Kona low frequency in the central
97 Pacific, suggesting that with the jet exit region retracted west of its climatological
98 position near the dateline, the waveguide was absent north of the Hawaiian Islands,

consequently allowing unimpeded equatorward propagation of extratropical disturbances to the subtropics in that longitude sector.

More recently, the studies of Athanasiadis et al. (2010) and Jaffe et al. (2011) identified two leading modes of variability of the North Pacific jet. Both studies employed EOF analyses of unfiltered zonal wind data and found the leading mode consisted of a longitudinal shift of the North Pacific jet exit region such that in the extended phase (EOF 1+) the jet reached as far eastward as the west coast of North America, while in the retracted phase (EOF 1-) the jet extended only as far as 160°E. The second mode highlighted a 10-15° meridional shift in the jet exit region (EOF 2+, a northward shift; EOF 2-, an equatorward shift). Jaffe et al. (2011) also investigated the synoptic evolution of sudden jet retractions and found the characteristic timescale for such events was ~10 days.

Thus, of the four characteristic North Pacific jet configurations associated with the leading two modes of variability (EOF 1+, EOF 1-, EOF 2+, and EOF 2-), only the synoptic-evolution of jet retractions (EOF 1-) has been investigated. That investigation (by Jaffe et al. 2011) was undertaken by compositing on a single time of maximum jet retraction. Employment of such a method limits the ability of the composite to capture the temporal evolution of associated large- and synoptic-scale structures.

In order to enhance the degree of temporal coherency in the construction of composites, a robust method of identifying and describing the evolution of the jet stream structure is required. This paper adapts the extended EOF methodology (e.g. Weare and Nasstrom 1982, Wilks 2011) to examine the synoptic evolution of

122 temporally coherent structures characterizing the leading modes of North Pacific jet
123 variability. A description of the time-extended EOF (TE-EOF) method, along with
124 details of its implementation in this study, is discussed as part of a broader
125 description of the methodology in Section 2. Section 3 describes the jet variability on
126 synoptic timescales within the TE-EOF framework. Time-lagged composites,
127 constructed based on the TE-EOF analysis, highlighting synoptic features both over
128 the North Pacific and associated with downstream impacts over North America are
129 presented in section 4. Additional time-lagged composites of anomalous deep
130 convection are constructed via the same methodology and presented in section 5. A
131 summary and suggestions for future work are discussed in section 6.
132

133 **2. Methodology**

134 EOF analysis is a statistical method by which the dominant modes of
135 variability that describe a multi-dimensional dataset are identified (e.g. Hannachi
136 2004, Wilks 2011). The patterns of greatest interest in an EOF analysis are those
137 that explain the largest fraction of variability within that dataset. In the atmosphere,
138 EOF analyses provide insight into the primary modes of variability associated with a
139 particular atmospheric variable over a pre-defined spatial region and period of time.
140 Use of EOF analyses has led to the identification and analysis of large-scale patterns
141 in the atmosphere (e.g. the PNA, Wallace and Gutzler 1981; AO, Thompson and
142 Wallace 1998), although not all EOFs have a meaningful physical interpretation.
143 Given that each mode of variability identified by an EOF analysis is defined to be
144 statistically independent of all other modes, changes in any one mode have no

correlation with changes in any other mode. In complex systems, such as the atmosphere, the asserted mathematical independence of each mode need not be mirrored in reality. The approach taken here is to apply physical insight with this statistical approach (EOF analyses) to develop understanding that neither the physics nor statistics might provide alone.

The traditional EOF analyzes a temporal sequence of spatial information to determine patterns of spatial co-variability without providing any sense of how such a pattern may evolve through time. By extending the input data to include a temporal dimension, EOF analysis can identify the time-dependent evolution of spatial patterns. This particular extended EOF (Weare and Nasstrom 1982, Wilks 2011) has been termed a time-extended EOF (TE-EOF; Roundy and Schreck 2009) and describes the leading modes of spatial-temporal evolution for the analyzed data. TE-EOF incorporates temporal variability by analyzing a number of times either side of a central reference time. By doing so, temporal data is incorporated into the TE-EOF twice – once as a way to maintain the coherence of data related to the evolution of the pattern over a, for instance, 10-day window (the additional TE-EOF dimension, termed a "TE window") and once as the time series over which to calculate the eigenmodes and identify the patterns (or, for TE-EOFs, the temporal evolutions) associated with each mode of variability. Weare and Nasstrom (1982) introduced the concept of extended EOF analysis in the atmospheric sciences and emphasized the utility of extended EOFs that incorporate additional temporal data due to the "significant auto- and cross-correlations in time" associated with the similarity of atmospheric data (specifically the broad similarities shared by any two

consecutive atmospheric states). Extended EOFs have been utilized to produce multivariate extended EOF analyses (calculated with multiple variables instead of multiple times), such as those used by Wheeler and Hendon (2004) to monitor the Madden-Julian Oscillation, and the time-extended EOF analyses used to forecast organized modes of tropical convection by Roundy and Schreck (2009).

The TE-EOF analyses performed in this study were constructed using 31 years (1980-2010) of data from the NCEP/NCAR Reanalysis (Kalnay et al. 1996) with data at 2.5° horizontal grid spacing and 6-hourly resolution. This data provides an EOF analysis of comparable quality to one constructed from an analysis with finer horizontal resolution such as the Climate Forecasts System Reanalysis (CFSR; Saha et al. 2010), but at substantially reduced cost. Zonal wind at the 250-hPa level (i.e. the jet level) was used at each analysis time throughout the winter months of November – March (NDJFM) in the 31 seasons. The chosen spatial domain of 100°E–120°W and 10°N–80°N allows sufficient space around the entrance and exit regions of the North Pacific jet stream in order to fully capture the variability directly associated with each. The TE-EOFs are performed over a TE-window of 40 time steps (10 days) using zonal wind anomalies beginning at each 6-hourly time step during NDJFM. These times are buffered by five days at the beginning of November and end of March to include only 10-day TE windows that fall completely within the NDJFM period. For example, the first (second) TE window in this analysis extends from 0000 UTC 1 Nov to 1800 UTC 10 Nov (0600 UTC 1 Nov to 0000 UTC 11 Nov) and is represented by the central time (referenced as D0) of 0000 UTC 6 Nov (0600 UTC 6 Nov).

In constructing the TE-EOF analyses, tests were performed to examine the sensitivity of the resulting TE-EOF 1 and TE-EOF 2 patterns to the chosen temporal and spatial constraints on the domain. Given the broad similarity of DJF and NDJFM zonal wind EOFs (not shown), and in order to reduce calculation time, the TE-EOFs for the sensitivity tests were calculated only over the DJF period. To test temporal constraints, the TE window length was varied from 6 days to 16 days, revealing only minor changes in the TE-EOF patterns. Numerous variations of the spatial domain were tested, both increasing and decreasing the extent in all directions. Expansions of the domain captured the large zonal wind variability associated with other climatological jet streams over central Asia and eastern North America, but did not significantly impact the pattern over the North Pacific. The spatial dimensions of the domain specified above were therefore chosen to focus on variability of the North Pacific jet while excluding other remote regions of high zonal wind variability. Tests were also performed to determine the separation of the leading EOFs in accordance with the method detailed by North (1982), and the first two EOFs are well separated.

The utility of the TE-EOF methodology is evident when comparing the resultant principal components (PCs) to the PCs of a traditional EOF analysis on the same data. PCs represent a measure of how well the data at a given time project back onto a given mode of variability. A time series of PCs provides a running measure of this projection and is standardized to aid interpretation. For the NDJFM months of 2009-2010, Fig. 1 compares the TE-PC (from a 10-day TE window) to the traditional PC (instantaneous; calculated every 6 h) and the 10-day centered

214 running mean of the traditional PC. While the traditional PC captures more
215 variability of the state of the North Pacific jet stream on short time scales, since this
216 PC is constructed with data from an individual time it is not designed to maintain
217 temporal coherence and appears noisy at times. Smoothing the traditional PC time
218 series over 40 points (10 days) provides values that appear similar to, but are
219 generally of smaller magnitude than, the TE-PC values. As a result, the TE-PC better
220 captures the full magnitude of highly anomalous events on the 10-day timescale
221 while eliminating much of the noise from higher-frequency variability, facilitating a
222 focus on events on the synoptic time scale. While Fig. 1 contains data only for the
223 2009-2010 NDJFM season, similar comparisons hold across all winters since 1980-
224 1981 and suggest the TE-EOF methodology is well suited for identifying
225 intraseasonal shifts in the structure of the North Pacific jet stream as suggested by
226 previous studies of North Pacific jet variability (e.g. Jaffe et al. 2011)

227 It is important to note that the TE-EOF modes are defined in a manner that
228 does not require that peaks in a PC from a traditional EOF technique correspond to
229 peaks in a mode from the TE-PC. The TE-PC captures the broader evolution of the
230 pattern without accounting for higher-frequency signals that may project onto the
231 traditional EOF patterns yet lack temporal longevity. It is likely these types of peaks
232 in the PC are not captured by the TE-EOF and may account for some of the lower
233 percent of variance explained with each TE mode when compared to the
234 corresponding traditional EOF over the North Pacific region[1]. Such a reduction in

[1]The percent variance explained in Jaffe et al. (2011) for EOF 1 is 15.9%, compared to our 9.1%. Our TE-EOFs are calculated using approximately 40 times the number of data points than used in a traditional EOF analysis.

explained variance by a given TE-EOF is related to the larger number of data points employed in the construction of the TE-EOF, providing increased variability for which to potentially account (Weare and Nasstrom 1982).

In order to supplement the TE-EOF analysis of the zonal wind field with physical analysis, we constructed composite analyses of high-amplitude events (those with normalized anomalous magnitudes exceeding 1.5 standard deviations) in the TE-PC time series during NDJFM for the years 1980–2010[2]. These composites were constructed with anomalies calculated by subtracting a 21-day centered running mean of gridded data from the NCEP/NCAR Reanalysis (Kalnay et al. 1996), the same dataset used to perform the TE-EOF analyses. Such composites allow for an examination of the synoptic-scale patterns preceding and following high-amplitude peaks in given modes of jet stream variability. In addition, outgoing longwave radiation (OLR) anomalies from the NOAA Interpolated OLR dataset (Liebmann and Smith 1996) were utilized in constructing additional composite analyses in order to serve as a reasonable proxy for anomalous cloud cover and convection in the tropics and subtropics. These data allow for identification of relationships between tropical/subtropical convection and the leading modes of zonal wind variability. In all composites, D0 will refer to date and time where a local maximum (or minimum) in the given TE-PC exceeded the prescribed threshold, while D-5d and D+5d will (as two examples) refer to the dates five days prior to and five days following D0, respectively.

[2] All cases within each category are well separated and so can be considered independent events.

3. Preferred modes of variability

The TE-EOF analyses presented here remain consistent with the leading modes of jet stream variability identified by previous work while explicitly incorporating the temporal evolution of synoptic-timescale patterns in the North Pacific jet stream into the analyses. Previous work has shown the spatial patterns associated with the leading modes of variability of the zonal wind over the North Pacific (e.g. Fig. 4 of Athanasiadis et al. 2010, Fig. 4 of Jaffe et al. 2011) to be similar to the patterns associated with the two leading modes of variability found at the central day (D0) of the TE-EOF analysis as shown in Fig. 2 (TE-EOF 1) and Fig. 3 (TE-EOF 2). The two other panels of Figs. 2 and 3, labeled as D-5d and D+5d, represent the beginning and end of the TE window, respectively. It is important to recognize that the sign associated with any EOF analysis is arbitrary and the signs of the TE-EOFs presented here have been chosen in a manner consistent with previous literature.

TE-EOF 1 is comprised of zonal wind variability along the latitude of the climatological jet core (~35˚N), with the mode's primary center of action located in the exit region of the climatological jet. Figure 2 presents the zonal wind anomalies from the NCEP/NCAR Reanalysis regressed back onto the TE-EOF pattern, resulting in a maximum anomaly in excess of 24 m s^{-1} at D0 (Fig. 2b). This anomaly represents the extension (when positive) and retraction (when negative) events of the North Pacific jet characterized by TE-EOF 1. A second set of anomalies of the opposite sign can be found both poleward and equatorward of the maximum anomaly in the jet

exit region. In general, the large-scale TE-EOF anomalies maximize in intensity near the central time of the 10-day TE window (D0).

TE-EOF 2 represents a meridional shift in the exit region of the climatological jet stream, described by a pair of anomalies of opposing sign straddling the climatological axis of the jet stream (Fig. 3). Such a pattern indicates a shift of the zonal wind to the flank of the climatological jet exit region. The northern (southern) anomaly center, when positive, represents a poleward (equatorward) shift in the jet exit region. These distinct shifts correspond, respectively, to the positive and negative phases of TE-EOF 2.

4. Composite analysis

In order to provide insight into the evolution of the synoptic-scale patterns associated with each phase of the two modes of variability, four separate composites were constructed. Each instance in which a given PC's value reached a local maxima or minima in excess of ±1.5 standard deviations was selected for the composite. Anomaly data from upper (250 hPa) and lower (850 hPa) levels at the selected times were averaged to produce each composite. The same NCEP/NCAR Reanalysis anomaly data described in section 2, and used to originally construct the TE-EOFs, were also employed in the construction of the composites.

a. Extension (positive TE-EOF 1)

The composite analysis of positive TE-EOF 1, created from 40 individual maxima in the PC of TE-EOF 1, is presented in Figure 4. This positive phase

represents an extension of the climatological jet over the North Pacific, with the strongest zonal wind anomaly at D0 located near 35˚N and 165˚W (Fig. 4c), firmly embedded within the exit region of the climatological jet. At upper levels, a negative height anomaly in the central North Pacific at D-10d (Fig. 4a) supports a 10 m s^{-1} zonal wind anomaly on it southern flank in the exit region of the climatological jet. Strengthening to 15 m s^{-1} by D-5d (Fig. 4b), the zonal wind anomaly extends from 150˚E to 140˚W while remaining equatorward of an upper level negative height anomaly and its companion low-level anomaly (Fig. 4g) south of the Aleutian Islands. The low-level height anomaly, indicative of a cyclone, is supported at upper levels by its location in the poleward exit region of the extended jet, a region favorable for cyclone development.

Near the Asian coast at D-10d (Fig. 4a), a separate negative height anomaly supports an enhancement of the wind speeds on the anticyclonic shear side of the climatological jet. This enhancement strengthens and zonally elongates by D-5d (Fig. 4b), increasing upper-level flow out of the tropics near the Asian coast. Over time, this feature merges with the broader negative height anomaly in the central North Pacific (Fig. 4c, d). There, the anomalous height differential (over 300 m) between 20˚N and 40˚N is greatest at D0 and is tied to a zonal wind anomaly of ~30 m s^{-1}, effectively doubling the zonal wind in this jet exit region (Fig. 4c). The enhancement of the zonal wind in the jet exit region extends the climatological jet 20˚ farther east, approaching the west coast of North America by D+5d (Fig. 4d). This jet naturally follows the southern edge of the negative height anomaly in the central Pacific. Beneath the upper height anomaly, the 850-hPa cyclone continues to develop (-180

m minimum height anomaly) and maintains its position in the poleward exit region of the extended jet as both shift eastward (Fig. 4f-h). By D+5d, the upper feature remains sprawling and moves the jet even farther east (Fig. 4d) before weakening and returning to the central North Pacific by D+10d (Fig. 4e). Accordingly, the 850 hPa anomalous heights begin to shift onshore over western North America (Fig. 4i), indicating the low-level cyclonic anomaly is increasingly impacting the sensible weather over North America.

It is interesting to note that the height and zonal wind anomalies over eastern Asia at D-5d, particularly those associated with the dipole of positive heights near over central Siberia and negative heights near the Korean peninsula, weaken through D0 and are essentially absent by D+5d. The fact that the intensity of each peaks early in the TE window suggests that this dipole may be a precursor to jet extension events over the North Pacific. This couplet is also represented in the 850 hPa temperature anomalies, with anomalous warmth over central Siberia and anomalous cold (in excess of -3˚C) over eastern China at D-5d (Fig. 4g).

Downstream over North America, height anomalies start to amplify by D0, with positive height anomalies at 250 hPa over western Canada (Fig. 4c) associated with 850 hPa temperature anomalies in excess of 2˚C (Fig. 4h). Farther downstream over the eastern portion of the United States and maritime Canada, negative height anomalies develop (Fig. 4c) in association with a small region of low-level cold anomalies in excess of -2˚C at D0 (Fig. 4h). The anomalously low heights over eastern North America support an enhancement of the upper jet on the anomaly's equatorward edge, resulting in a stronger subtropical jet over the southeast United

States and a pattern that resembles the positive Pacific North America (PNA) teleconnection pattern (Horel and Wallace 1981, Wallace and Gutzler 1981). While the upper height and low-level cold anomalies slowly slide southeastward through D+5d, the warm anomalies intensify and expand over much of the western half of North America, peaking in excess of 4˚C (Fig. 4i). This widespread warmth remains at D+10d (Fig. 4j), but only a few small areas are statistically significant at the 95% level.

b. Retraction (negative TE-EOF 1)

Composites of the jet retraction cases (negative phase of TE-EOF 1) were constructed from 40 times in which the PC peaked below the -1.5 standard deviation threshold (Fig. 5). While composites associated with the negative phase of TE-EOF 1 are not statistically required to be mirror opposites of the positive phase of TE-EOF 1 (due to the varying amplitudes of the cases used in the composite mean), the large-scale structures describing the two phases tend to exhibit this characteristic.

At upper levels at D-10d (Fig. 5a), small positive height anomalies are located in the central North Pacific just north of the exit region of the climatological jet, supporting a small ~10 m s^{-1} negative zonal wind anomaly in the exit region. By D-5d (Fig. 5b), this region of anomalous heights south of the Aleutians intensifies substantially and expands along the entire northern flank of the climatological North Pacific jet. The core of the negative zonal wind anomalies is located near 180˚, resulting in a retraction of the jet to west of the date line. Negative zonal wind

anomalies peak at D0 in excess of -30 m s^{-1} with these cases (Fig. 5c) in a region where the climatological wind is only ~45 m s^{-1}. Centers of enhanced zonal winds exist both poleward and equatorward of the climatological jet stream with the positive zonal wind anomaly stronger on the poleward side. A modest upper-level neative height anomaly appears west of Hawaii at D-5d (around 20˚N and 180˚ longitude; Fig. 5b) and exists throughout the 10-day TE window, expanding eastward by D0. Anomalous cyclonic flow around this feature provides additional support for a reduction in climatological westerlies in the jet exit region.

East Asian precursors are comparable but roughly opposite those of the jet extension mode (Fig. 4b, g and 5b, g). Most of Siberia is dominated by sprawling negative height anomalies at upper-levels (Fig. 5a, b) and associated low-level cold anomalies (below -4˚C; Fig. 5f, g), while east-central China and the Sea of Japan are dominated by a western lobe of the positive height anomaly feature that spreads eastward and consolidates with time in the 10-day TE window (Fig. 5b-d). The anomalously cold air, largely in Siberia initially (Fig. 5g), spreads eastward to encompass Alaska and western Canada where anomalous cold exceeds -5˚C by D0 (Fig. 5h).

The downstream patterns are of similar amplitude (though of greater statistical significance) and evolve comparably to those observed in jet extension composites, but are again of reversed sign (Fig. 4d, i and Fig. 5d, i). A broad region of anomalously low heights at 850 hPa can be seen sliding out of the Arctic Ocean around D0 (Fig. 5h) and into western Canada by D+5 (Fig. 5i), drawing cold air into Alaska for at least 10 days after peak retraction (Fig. 5h-j). While the low-level

394 negative height anomalies over North America disappear by D+10d (Fig. 5j), the
395 upper level height anomaly dipole remains significant over the central Pacific and
396 the anomalous zonal wind magnitude remains above 15 m s^{-1} beyond D+10d.
397
398 *c. Poleward shift (positive TE-EOF 2)*
399 Two primary centers of action straddling the mean jet exit region dominate
400 the 10-day composite analyses of 36 poleward shifted jet cases (cases exceeding
401 +1.5 standard deviations of TE-EOF 2). A strip of positive zonal wind anomalies
402 north of the climatological jet axis and negative anomalies south of the
403 climatological jet axis serves to shift that climatological jet poleward, from as far
404 west as western China at D-10d (Fig. 6a) to the northwest US beyond D0 (Fig. 6c, d).
405 The strongest zonal wind anomalies are predominantly located poleward of the jet
406 exit region.
407 A poleward shift of the jet similarly shifts the synoptic-scale height anomaly
408 centers 10-15˚ poleward of the climatological jet axis. A zonally elongated positive
409 height anomaly centered near the latitude of the climatological jet core but in the jet
410 exit region (Fig. 6a) contrasts with a broad negative height anomaly over the Gulf of
411 Alaska and far eastern Russia by D-5d (Fig. 6b), helping to shift the pattern
412 poleward and intensify the jet between the height anomalies. The negative height
413 anomaly and its associated low-level cyclonic anomaly retrograde across the
414 Aleutian Islands and weaken from D0 through D+10d (Fig. 6c-e). The weakening of
415 the negative upper-level height anomaly is coincident with an amplification of the
416 positive height anomalies over Hudson Bay by D+5d (Fig. 6d). While there are no

significant temperature anomalies associated with the anomalous low-level cyclonic feature near the Aleutians before D-5d (Fig 6f, g), the anomalous tropospheric deep cyclonic flow enhances the low-level cold (warm) temperature anomalies present over the Bering Sea (central Canada; Fig. 6h-j). While the cold temperature anomalies over far eastern Russia peak in excess of -4˚C at D+5d (Fig. 6i), the corresponding warm anomalies over central Canada appear to be enhanced by southwesterly winds downsloping off the Rocky Mountains into Prairie Canada and peak in excess of +8˚C at D+5d. This anomalous warmth continues to impact northeastern North America at D+10d (Fig. 6j), although the statistically significant portion of these anomalies becomes limited.

Upstream of the North Pacific, a weak and nearly stationary region of positive height anomalies is present near the entrance region of the climatological jet at 110˚E (D-10d, Fig. 6a). This feature is maintained throughout the 20 day composite, suggesting its presence may be related to a persistent forcing such as deep convection. If so, its presence at D-10 and D-5d may prove to be a key precursor feature for poleward shifted jet events.

d. Equatorward shift (negative TE-EOF 2)

The upper-level zonal wind pattern associated with the equatorward shift mode (negative phase of TE-EOF 2) is more challenging to interpret than the composites associated with the previously discussed phases. The primary zonal wind anomalies in the composite straddle the climatological jet exit region with enhanced westerlies located on the southern periphery with a stronger region of

reduced westerlies to the north prior to and throughout the 10-day window (Fig. 7a-d). This structure is similar to but opposite that of the positive phase of TE-EOF 2 and is termed "equatorward shift." While such a description allows for a convenient consistency in nomenclature, poleward shifted jet events are not characterized by negative zonal wind anomalies in a similar location (Fig. 6b-d), providing a notable asymmetry between the positive and negative phases of TE-EOF 2. We note that the anomalous enhancement of upper-level zonal winds over Alaska and eastern Russia in this composite is of equal or greater magnitude than the enhanced westerly flow in the subtropics and may instead represent an associated invigoration of the polar jet stream (Fig. 7b-d).

The equatorward shift mode is comprised of anomalous westerly zonal wind along 20˚N latitude in the central Pacific throughout the composite, with the maximum westerly anomaly over the Hawaiian Islands (Fig. 7a-d). This anomalous jet extends eastward from its D-5d position (Fig. 7b) and connects with an anomalous wind speed maximum over central North America, creating a link between the enhanced equatorward-shifted subtropical Pacific jet and the climatological jet stream over Mexico and the United States at D0 and D+5d (Fig. 7c, d). A broad region of negative height anomalies over the western United States and central Canada acts in concert with a less intense positive height anomaly feature in the southeast United States to enhance the upper winds between the anomaly centers. The upper cyclonic anomaly is associated with remarkable cold anomalies in excess of -8˚C at 850 hPa over much of Canada (Fig. 7f-h). The magnitude of these anomalies increases dramatically as they become statistically significant between D-

463 5d and D0 (Fig. 7f, g). Though the underlying physical mechanism driving these local
464 temperature tendencies is not immediately clear, some of the local temperature
465 decrease is likely associated with cold air advection in northwesterly low-level flow
466 over Alaska and northwestern Canada stemming from the intensifying low-level
467 anticyclonic anomaly over the Aleutian Islands (Fig. 7f-h).

468 Over the central North Pacific, a broad region of substantial upper-level
469 positive height anomalies north of 40˚N enhances the jet stream on its poleward
470 flank, north of 60˚N (Fig. 7b-d). The cross-arctic flow associated with such a jet is
471 also represented at the 850-hPa level and likely contributes to the anomalous low-
472 level cold in North America at D0 and D+5d (Fig. 7g, h). South of this upper-level
473 feature, a broad region of anomalously low heights is present south of the
474 climatological jet near its exit region and may represent broad upper troughs
475 digging into the subtropics across a range of longitudes in a manner similar to that
476 observed in jet retraction cases (e.g. Fig. 5a-e). The position suggests a connection
477 to the Kona lows that occur in conjunction with retracted jet cases (e.g. Otkin and
478 Martin 2004) as any such disturbance may slightly enhance the subtropical jet south
479 of its associated trough.

480 The upstream patterns over Asia are diffuse with no clear-cut synoptic-scale
481 anomalies from D-10d to D0 at upper levels (Fig. 7b, c). This suggests that either the
482 equatorward shift mode is triggered by well-defined but opposing synoptic-scale
483 setups that are washed out in a composite mean analysis or that there are not any
484 clear cut Asian mid-latitude precursors to these events.
485

5. Tropical convection composites

Although some results from the poleward shifted jet composite suggested a connection to tropical convection, specifically the building of low-latitude anomalous ridges, such inferences are unsupported without examining proxies of the convection itself. Jaffe et al. (2011) performed such composites for retracted jet cases, finding a quasi-stationary convective signal both before and after a jet retraction event. Figures 8 and 9 present OLR composites calculated as discussed in section 4 for each phase of each TE-EOF. OLR is often utilized as a proxy for cold cloud tops associated with deep convection in the tropics and subtropics and is useful in the construction of composites due to its long, homogenous period of record. The OLR composites for the retraction mode (Fig. 8b, d, f) and the poleward shift mode (Fig. 9a, c, e) show apparent large-scale organization of anomalous enhanced tropical convection.

Anomalous tropical convection appears in the retraction composite over the eastern Indian Ocean and Maritime Continent (Fig. 8b, d, f) and appears to move slowly eastward throughout the 10-day window of the composite. The eastward phase speed of this convection appears similar to or slightly slower than that of convection associated with the Madden-Julian Oscillation (MJO; Madden and Julian 1972, Zhang 2005), which contrasts with the stationary nature of convection found with the retraction mode in Jaffe et al. (2011). The role of this convection in fostering a retraction of the North Pacific jet is not immediately apparent. A separate region of convection in the central and eastern tropical North Pacific is consistent with the OLR composite from Jaffe et al. (2011; specifically their Day 10 composite

509 [their Fig. 12e] and our D+5d; Fig. 8f) near the Hawaiian Islands, although twice as
510 intense as that found by Jaffe et al. Convection in this location is consistent with the
511 presence of the low-latitude trough that can be inferred from the retraction
512 composites (Fig. 5b-d). Notably, the distribution of convection prior to the mature
513 phases of EOF 1 (Figs. 8a, b) does not correspond to that associated with the
514 positive/negative PNA evolutions illustrated in Franzke et. al (2011) (their Fig. 11).
515 Significant tropical convection anomalies are evident in the poleward shift
516 composite (Fig. 9a, c, e) over Southeast Asia and the Maritime Continent and are of a
517 larger magnitude than those observed in a similar location in association with the
518 retraction mode. These negative OLR anomalies also appear to remain nearly
519 stationary or move slowly eastward similar to convection associated with the MJO.
520 It is interesting to note that these convective anomalies move eastward at
521 approximately the same speed as the anomalies associated with the retracted jet
522 events (Fig. 8b, d, f), roughly 2˚ per day. The quasi-stationary or slow-moving nature
523 of these convective anomalies enables the imposition of persistent forcing on the
524 mid-latitude flow patterns which can impact both the North Pacific jet as well as
525 locations downstream (e.g. Hoskins and Karoly 1981, Kiladis and Weickmann 1992,
526 Higgins et al. 2000). Downstream impacts are commonly realized via the excitation
527 of waves along the upper-level waveguide, or jet (e.g. Gill 1980, Simmons 1992,
528 Martius 2010), especially when the convection is located ~10-20˚N of the equator as
529 it is in these composites analyses. The broad low-latitude upper-level positive
530 height anomalies in the entrance region of the poleward shift composite (Fig. 6a-e)

may be a manifestation of upper-level convective outflow in this location that appears to make systematic contributions to the poleward shift of the jet.

Finally, it is worth noting that the large region of anomalously high OLR in the eastern Pacific on the equatorward side of the extended jet's exit region (Fig. 8 a, c, e) is coincident with the subsiding branch of the thermally indirect circulation associated with the extended jet. This OLR anomaly intensifies throughout the 10-day composite (Fig. 8c, e). Farther north, the rising branch of the thermally indirect circulation likely enhances convection in the region of anomalously low OLR off the west coast of the United States at D0 (Fig. 8c).

6. Discussion

TE-EOF analysis reveals the details of the synoptic-scale evolutions associated with the leading modes of North Pacific jet stream variability. While the TE-EOF analysis presented here is consistent with the leading modes of variability previously presented by Schubert and Park (1991), Athanasiadis et al. (2010), and Jaffe et al. (2011), the TE-EOF analysis provides an additional component of temporal coherence to analyses of the large-scale environments characteristic of extremes in the leading modes of variability, and thus points to both upstream precursors and downstream impacts.

The two primary modes of variability presented here consist of 1) the jet in either an extended or retracted state or 2) a poleward or equatorward shift of the jet exit region. While previous studies of North Pacific jet variability focused on the transition into a retracted state (Jaffe et al. 2011) and the instantaneous state of the

554 jet in any given mode (Athanasiadis et al. 2010), the TE-EOF technique identifies the
555 evolution of the two phases of each mode of variability centered on the peak
556 intensity of each phase. By design, the extension/retraction and latitudinal shift
557 modes reach their greatest extents at D0 and so employment of the TE window,
558 which includes some of the growth of the zonal wind anomalies toward (and decay
559 away from) such peaks, reveals new details regarding the corresponding flow
560 evolutions.

561 Composites constructed based upon high-amplitude events in the TE-PC time
562 series constitute an improvement in the temporal coherence of the associated mid-
563 latitude signals compared to composites constructed with traditional EOFs (e.g. Jaffe
564 et al. 2011). The development of the positive zonal wind anomalies throughout the
565 TE window for the extended jet mode (Fig. 4) draws attention to the role of the
566 negative height anomaly that intensifies and moves eastward throughout the
567 following 10 days (Figs. 4a-e). This feature, suggestive of an upper trough, appears
568 to be central to the development and intensification of the zonal wind anomalies
569 that constitute an extended jet stream and is a central component of the synoptic
570 evolution of the positive phase of the PNA pattern as described by Franzke et al.
571 (2011). Expanding these composite analyses farther back in time may allow for
572 better identification of such precursor features and their evolution over several
573 days prior to the central time of the TE window. Forward extension of such analyses
574 may provide additional insights into the subsequent evolution of high-amplitude
575 events for all four phases of jet variability. The analysis suggests that, armed with a
576 physical understanding of the precursors that drive changes in the North Pacific jet,

577 medium-range forecasters may be better able to combine an anticipation of jet
578 variability with the additional knowledge of the associated downstream impacts to
579 improve large-scale forecasts into week two over much of North America.

580 Prior work by Otkin and Martin (2004) and Jaffe et al. (2011) has shown that
581 the evolution of EOF 1 is broadly similar to the synoptic evolution of the PNA
582 pattern. Consequently, they suggested that jet retraction and extension may be
583 governed by some of the same physical processes as the growth of the
584 positive/negative PNA patterns. In their analysis of the synoptic evolution of the
585 PNA, Franzke et. al (2011) show that convection is enhanced (weakened) over the
586 western tropical Pacific and weakened (enhanced) over the tropical Indian Ocean, in
587 association with the initial development of the positive (negative) PNA pattern.
588 Such a distribution does not characterize the two phases of EOF 1 presented here.
589 This fact suggests that the physical factors influencing the evolution of the PNA,
590 though similar in some respects, are different in some meaningful way from those
591 that alternately extend and retract the jet.

592 The composite analyses of extended jets (Fig. 4) are, at certain times,
593 consistent with the low-level evolution of the surge phase of the East Asian Winter
594 Monsoon (EAWM; Chang and Lau 1980). For instance, at D-5d of the extended jet
595 composite (Fig. 4g), the large area of anomalous low-level cold air over eastern
596 China and the northern South China Sea is in a location consistent with the
597 composite cold surge described by Chang and Lau (1980). Such cold air outbreaks
598 were also identified as a possible precursor to jet extension events by Jaffe et al.

599 (2011) and may play a role in the evolution of extended jets as recently suggested
600 by Handlos and Martin (2016).

601 Within these composite analyses, consistent high-amplitude impacts were
602 noted downstream over North America in the days after the peak in the respective
603 jet mode. For TE-EOF 1, the jet extension (retraction) mode is associated with a
604 large region of low-level warmth[3] (cold) over much of Alaska and western Canada at
605 D0 (Fig. 4h, 5h), with temperature anomalies in excess of 4˚C magnitude. These
606 anomalies suggest such weather might be a common downstream impact of each
607 EOF 1 phase. Similarly, the phases of TE-EOF 2 are associated with even stronger
608 downstream impacts over North America, with both poleward and equatorward
609 shift events leading to low-level temperature anomalies in excess of 8˚C. Neither of
610 these anomalies are of high magnitude prior to D-5d (Fig. 6g, 7f), but rather
611 intensify over North America as the shift of the jet exit region maximizes (at D0).
612 High magnitude temperature anomalies are maintained through D+5d (Fig. 6i, 7h)
613 and up to an additional five days after the poleward shift (Fig. 6j), suggesting that
614 latitudinal shifts of the jet exit region (TE-EOF 2) may affect the downstream
615 weather over North America more significantly than jet extensions or retractions
616 (TE-EOF 1).

617 A similar suggestion was made by Linkin and Nigam (2008) in their
618 examination of the north Pacific Oscillation – west Pacific (NPO/WP) teleconnection
619 pattern – a pattern whose upper tropospheric geopotential and lower tropospheric

[3] The areal extent of warm anomalies (statistically significant at the 95% level) associated with jet extensions is substantially smaller than the associated anomalies for jet retractions. However, the anomaly distributions for each species at less stringent significance levels are very similar.

620 temperature anomalies are similar to those characteristic of our EOF 2. That study
621 was focused solely on the mature phase structure of that mode. The details of the
622 synoptic evolution of *both* leading modes of jet variability afforded by the TE-EOF
623 analysis presented here provides a perspective from which a better understanding
624 of aspects of the broader north Pacific variability – particularly determination of
625 whether the jet is a driver of, or a response to, other fundamental aspects of that
626 variability – might be developed.

627 Of the four phases associated with the two modes of variability discussed
628 here, slow-moving and potentially organized tropical convection may play a
629 significant role in two of them. A more complete analysis of the mid-latitude and
630 tropical interactions that lead to these variations in the jet would serve to provide
631 additional insight into the forcing behind such patterns, but is beyond the scope of
632 this study. The task of identifying such tropical-extratropical interactions has been
633 addressed in cases of recurving TCs interacting with the jet stream (e.g.
634 Archambault et al. 2013), but remains a challenge for less organized episodes of
635 persistent deep convection, which is a substantially more common phenomenon
636 throughout the tropics and subtropics. The leading modes of jet variability broadly
637 describe the most common evolutions of the North Pacific jet stream, implying tht
638 the most common modes of tropical convection (e.g. garden-variety as well as MJO-
639 and ENSO-driven) may play a more frequent and significant role in modulating such
640 North Pacific jet variability.

641 Finally, since the analyses presented here are based upon identification of
642 the dates of *maximum* extension, retraction, and shift, the leading modes identify, for

643 instance, the state of the jet *being extended* rather than the *process of extension*.
644 Thus, the transitions to and from these leading modes, while partially addressed by
645 the lagged composite analysis, merit additional study. Similarities between the jet
646 extension and poleward shift composites (the 850 hPa Gulf of Alaska cyclonic
647 anomaly and downstream warmth; Figs. 4 and 6) and the jet retraction and
648 equatorward shift composites (the 850 hPa Gulf of Alaska anticyclonic anomaly and
649 downstream cold; Figs. 5 and 7) suggest that the leading modes, while
650 mathematically independent, are not physically independent. Thus, examination of
651 the nature of transitions between the phases of each mode promises additional
652 insight into the preferred evolutions of the North Pacific jet stream.
653

654 **7. Acknowledgments**

655 The authors would like to thank the National Science Foundation for its
656 support of this work via grant number AGS-1265182. OLR data was obtained from
657 the NOAA/OAR/ESRL PSD, Boulder, Colorado, USA, for 1979–2012 from
658 http://www.esrl.noaa.gov/psd/. All of the figures presented here were created
659 using the NCAR Command Language (NCL; NCAR 2015). Finally, the suggestions of
660 three anonymous reviewers have served to clarify the presentation of this research.
661
662
663

664 **References**

665 Archambault, H. M., L. F. Bosart, D. Keyser, and J. M. Cordeira, 2013: A Climatological
666 Analysis of the Extratropical Flow Response to Recurving Western North
667 Pacific Tropical Cyclones. *Mon. Wea. Rev.*, **141**, 2325–2346.
668 doi: http://dx.doi.org/10.1175/MWR-D-12-00257.1
669 Athanasiadis, P. J., J. M. Wallace, and J. J. Wettstein, 2010: Patterns of Wintertime Jet
670 Stream Variability and Their Relation to the Storm Tracks. *J. Atmos. Sci.*, **67**,
671 1361–1381. doi: http://dx.doi.org/10.1175/2009JAS3270.1
672 Chang, C-P., and K. M. W. Lau, 1980: Northeasterly Cold Surges and Near-Equatorial
673 Disturbances over the Winter MONEX Area During December 1974. Part II:
674 Planetary-Scale Aspects. *Mon. Wea. Rev.*, **108**, 298–312.
675 doi: http://dx.doi.org/10.1175/1520-
676 0493(1980)108<0298:NCSANE>2.0.CO;2
677 Chu, P., A. J. Nash, and F. Porter, 1993: Diagnostic Studies of Two Contrasting
678 Rainfall Episodes in Hawaii: Dry 1981 and Wet 1982. *J. Climate*, **6**, 1457–
679 1462. doi: http://dx.doi.org/10.1175/1520-
680 0442(1993)006<1457:DSOTCR>2.0.CO;2
681 Eichelberger, S. J., and D. L. Hartmann, 2007: Zonal Jet Structure and the Leading
682 Mode of Variability. *J. Climate*, **20**, 5149–5163.
683 doi: http://dx.doi.org/10.1175/JCLI4279.1
684 Franzke, C. S. B. Feldstein, and S. Lee, 2011: Synoptic analysis of the Pacific-North
685 America teleconnection pattern. *Quart. J. Roy. Meteor. Soc.*, **137**, 329-346.
686 Gill, A. E., 1980: Some simple solutions for heat-induced tropical circulation. *Quart. J.*
687 *Roy. Meteor. Soc.*, **106**, 447–462.

688 Handlos, Z. J., and J. E. Martin, 2016: Composite analysis of large-scale environments
689 conducive to west Pacific polar/subtropical jet superposition. *J. Clim*., **29**, (in
690 press).
691 Hannachi, A., 2004: A primer for EOF analysis of climate data. Available online at
692 http://www.met.reading.ac.uk/~han/Monitor/eofprimer.pdf.
693 Higgins, R. W., J-K. E. Schemm, W. Shi, and A. Leetmaa, 2000: Extreme Precipitation
694 Events in the Western United States Related to Tropical Forcing. *J.*
695 *Climate*, **13**, 793–820. doi: http://dx.doi.org/10.1175/1520-
696 0442(2000)013<0793:EPEITW>2.0.CO;2
697 Horel, J. D., and J. M. Wallace, 1981: Planetary-scale atmospheric phenomena
698 associated with the Southern Oscillation. *Mon. Wea. Rev*., **109**, 813-829.
699 Hoskins, B. J., and D. J. Karoly, 1981: The steady linear response of a spherical
700 atmosphere to thermal and orographic forcing. *J. Atmos. Sci*., **38**, 1179–1196,
701 doi:10.1175/ 1520-0469(1981)038,1179:TSLROA.2.0.CO;2.
702 Jaffe, S. C., J. E. Martin, D. J. Vimont, and D. J. Lorenz, 2011: A Synoptic Climatology of
703 Episodic, Subseasonal Retractions of the Pacific Jet. *J. Climate*, **24**, 2846–
704 2860. doi: http://dx.doi.org/10.1175/2010JCLI3995.1
705 Kalnay, E., and co-authors, 1996: The NCEP/NCAR 40-year reanalysis project. *Bull.*
706 *Amer. Meteor. Soc.*, **77**, 437–471. doi: http://dx.doi.org/10.1175/1520-
707 0477(1996)077<0437:TNYRP>2.0.CO;2
708 Kiladis, G. N. and K. M. Weickmann, 1992: Circulation anomalies associated with
709 tropical convection during Northern winter. *Mon. Wea. Rev.*, **120**, 1900–1923.

710 doi: http://dx.doi.org/10.1175/1520-
711 0493(1992)120<1900:CAAWTC>2.0.CO;2
712 Koteswaram, P., 1953: An analysis of the high tropospheric wind circulation over
713 India in winter. *Indian J. Meteor. Geophys.*, **4**, 13-21.
714 Lewis, J. M., 2003: Ooishi's Observation: Viewed in the Context of Jet Stream
715 Discovery. *Bull. Amer. Meteor. Soc.*, **84**, 357–369.
716 doi: http://dx.doi.org/10.1175/BAMS-84-3-357
717 Liebmann, B., and C. A. Smith, 1996: Description of a complete (interpolated)
718 outgoing longwave radiation dataset. *Bull. Amer. Meteor. Soc.*, **77**, 1275–1277.
719 Linkin, M. E., and S. Nigam, 2008: The north Pacific oscillation-west Pacific
720 teleconnection pattern: Mature-phase structure and winter impacts. *J. Clim*.,
721 **21**, 1979-1997.
722 Loewe, F., and U. Radok, 1950: A meridional aerological cross section in the
723 southwest Pacific. *J. Meteor.*, **7**, 58–65. doi: http://dx.doi.org/10.1175/1520-
724 0469(1950)007<0058:AMACSI>2.0.CO;2
725 Madden, R. A. and P. R. Julian, 1972: Description of Global-Scale Circulation Cells in
726 the Tropics with a 40–50 Day Period. *J. Atmos. Sci.*, **29**, 1109–1123.
727 doi: http://dx.doi.org/10.1175/1520-
728 0469(1972)029<1109:DOGSCC>2.0.CO;2
729 _____, and _____, 1994: Observations of the 40–50-day tropical oscillation. *Mon.*
730 *Wea. Rev.*, **122**, 814-837.
731 Mohri, K., 1953: On the fields of wind and temperature over Japan and adjacent
732 waters during winter of 1950–1951. *Tellus,* **5**, 340–358.

733 Namias, J. and P. F. Clapp, 1949: Confluence theory of the high tropospheric jet
734 stream. *J. Meteor.*, **6**, 330–336. doi: http://dx.doi.org/10.1175/1520-
735 0469(1949)006<0330:CTOTHT>2.0.CO;2
736 NCAR Command Language (Version 6.3.0) [Software]. (2015). Boulder, Colorado:
737 UCAR/NCAR/CISL/TDD. http://dx.doi.org/10.5065/D6WD3XH5
738 Newton, C. W., 1954: Frontogenesis and frontolysis as a three-dimensional process.
739 *J. Meteor.*, **11**, 449-461.
740 North, G. R., T. L. Bell, R. F. Cahalan, and F. J. Moeng, 1982: Sampling errors in the
741 estimation of empirical orthogonal functions. *Mon. Wea. Rev*., **110**, 699–706.
742 Otkin, J. A. and J. E. Martin, 2004: The Large-Scale Modulation of Subtropical
743 Cyclogenesis in the Central and Eastern Pacific Ocean. *Mon. Wea. Rev.*, **132**,
744 1813–1828. doi: http://dx.doi.org/10.1175/1520-
745 0493(2004)132<1813:TLMOSC>2.0.CO;2
746 Palmén, E., 1951: The role of atmospheric disturbances in the general circulation.
747 *Quart. J. Royal Meteor. Soc.*, **77**, 337-354. doi:
748 http://dx.doi.org/10.1002/qj.49707733302
749 Roundy, P. E., and C. J. Schreck III, 2009: A combined wave-number–frequency and
750 time-extended EOF approach for tracking the progress of modes of large-
751 scale organized tropical convection. *Quart. J. Royal Meteor. Soc.*, **135**, 161-
752 173.
753 Schubert, S. D. and C. Park, 1991: Low-Frequency Intraseasonal Tropical-
754 Extratropical Interactions. *J. Atmos. Sci.*, **48**, 629–650.

755 doi: http://dx.doi.org/10.1175/1520-
756 0469(1991)048<0629:LFITEI>2.0.CO;2
757 Simmons, A. J. (1982), The forcing of stationary wave motion by tropical diabatic
758 heating. *Quart. J. Royal Meteor. Soc.,* **108**, 503–534.
759 doi: 10.1002/qj.49710845703
760 Thompson, D. W. J., and J. M. Wallace, 1998: The Arctic oscillation signature in the
761 wintertime geopotential height and temperature fields. *Geophys. Research*
762 *Letters*, **25**, 1297-1300.
763 Wallace, J. M. and D. S. Gutzler, 1981: Teleconnections in the geopotential height
764 field during the Northern Hemisphere winter. *Mon. Wea. Rev.*, **109**, 784–812.
765 doi: http://dx.doi.org/10.1175/1520-
766 0493(1981)109<0784:TITGHF>2.0.CO;2
767 Weare, B. C., and J. S. Nasstrom, 1982: Examples of Extended Empirical Orthogonal
768 Function Analyses. *Mon. Wea. Rev.*, **110**, 481–485.
769 doi: http://dx.doi.org/10.1175/1520-
770 0493(1982)110<0481:EOEEOF>2.0.CO;2
771 Wheeler, M. C., and H. H. Hendon, 2004: An All-Season Real-Time Multivariate MJO
772 Index: Development of an Index for Monitoring and Prediction. *Mon. Wea.*
773 *Rev.*, **132**, 1917–1932. doi: http://dx.doi.org/10.1175/1520-
774 0493(2004)132<1917:AARMMI>2.0.CO;2
775 Wilks, D. S., 2011: Statistical methods in the atmospheric sciences. Academic Press,
776 676 pp.

Yeh, T., 1950: The circulation of the high troposphere over China in the winter of 1945-46. *Tellus*, **2**, 173–183.

Zhang, C., 2005: Madden-Julian Oscillation. *Rev. Geophys.*, **43**.

List of figure captions

Figure 1. Comparison of a traditional PC, a traditional PC with a 10-day smoother, and a TE-PC for the NDJFM 2009-2010 season for the leading mode (top) and second leading mode (bottom) of variability. PCs correspond to EOFs of 250 hPa zonal wind speed over the North Pacific.

Figure 2. TE-EOF 1 (extension/retraction) of the 250 hPa zonal wind over the North Pacific. EOF regressed back onto anomaly data is shaded (m s^{-1}; per color bar). Climatological zonal wind is contoured in black starting at 20 m s^{-1}. Top panel (D-5d) represents the TE-EOF pattern at the beginning of the 10-day TE window; middle panel (D0) represents the pattern halfway through the TE window; bottom panel (D+5d) represents the pattern at the end of the TE window.

Figure 3. As in Fig. 2 but for TE-EOF 2 (meridional shift) of the 250 hPa zonal wind over the North Pacific.

Figure 4. Composite of cases where PC of TE-EOF 1 was positive and was greater than 1.5 standard deviations, representing jet extension cases. D0 is defined as the midpoint of the 10-day window, where D-5d (D+5d) is the beginning (end) point. Left plots (a-e) show anomalies of 250 hPa zonal wind (shaded per color bar; only where statistically significant at 95% level) and heights (dashed every 50 m). Right

800 plots (f-j) include anomalies of 850 hPa temperature (shaded per color bar; only
801 where statistically significant at 95% level) and heights (dashed every 20 m). Height
802 anomalies in all plots are only significant within regional identified by stippling. All
803 plots show the climatological zonal wind in thin black contours starting at 30 m s^{-1}.
804 Composite sample size = 40.
805 Figure 5. As in Fig. 4 for cases where the PC of TE-EOF 1 was less than -1.5 standard
806 deviations, representing jet retraction cases. Composite sample size = 40.
807 Figure 6. As in Fig. 4 for cases where the PC of TE-EOF 2 was greater than 1.5
808 standard deviations, representing poleward shift cases. Composite sample size = 36.
809 Figure 7. As in Fig. 4 for cases where the PC of TE-EOF 2 was less than -1.5 standard
810 deviations, representing equatorward shift cases. Composite sample size = 45.
811 Unlike the previous composites, D+10d did not contain anomalies that appeared
812 both physically meaningful and statistically significant.
813 Figure 8. Composites of OLR (shaded, per color bar) calculated as in Fig. 4 and Fig. 5
814 for jet extension (a, c, e) and jet retraction cases (b, d, f), respectively, from TE-EOF
815 1. Heights at 250 hPa contoured as in Fig. 4. Numbers of cases are consistent with
816 the respective previous composites.
817 Figure 9. As in Fig. 8 for poleward shift (from Fig. 6; a, c, e) and equatorward shift
818 (Fig. 7; b, d, f) jet cases from TE-EOF 2. Heights at 250 hPa contoured as in Fig. 4.
819 Numbers of cases are consistent with the respective previous composites.
820

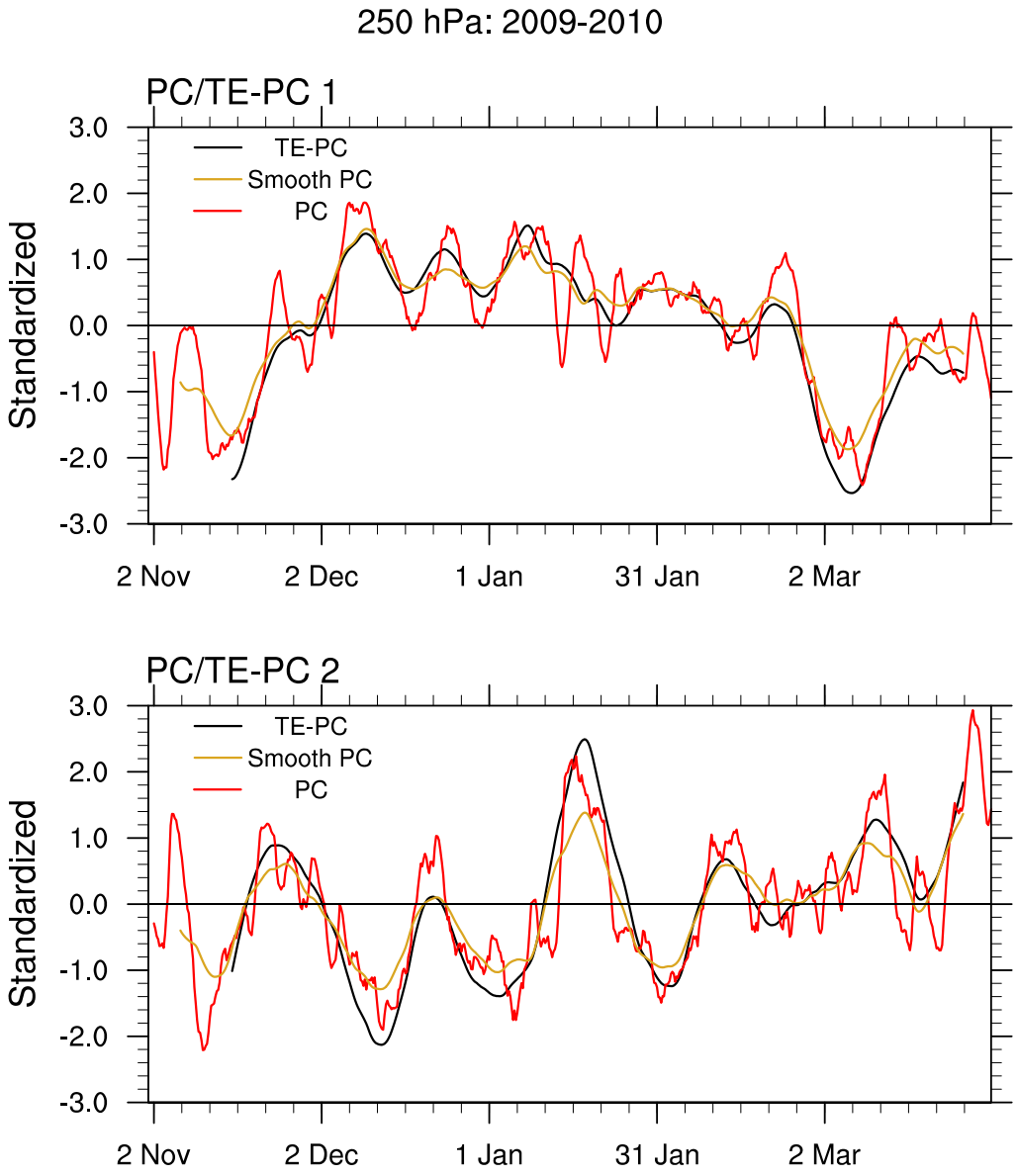

Figure 1. Comparison of a traditional PC, a traditional PC with a 10-day smoother, and a TE-PC for the NDJFM 2009-2010 season for the leading mode (top) and second leading mode (bottom) of variability. PCs correspond to EOFs of 250 hPa zonal wind speed over the North Pacific.

826

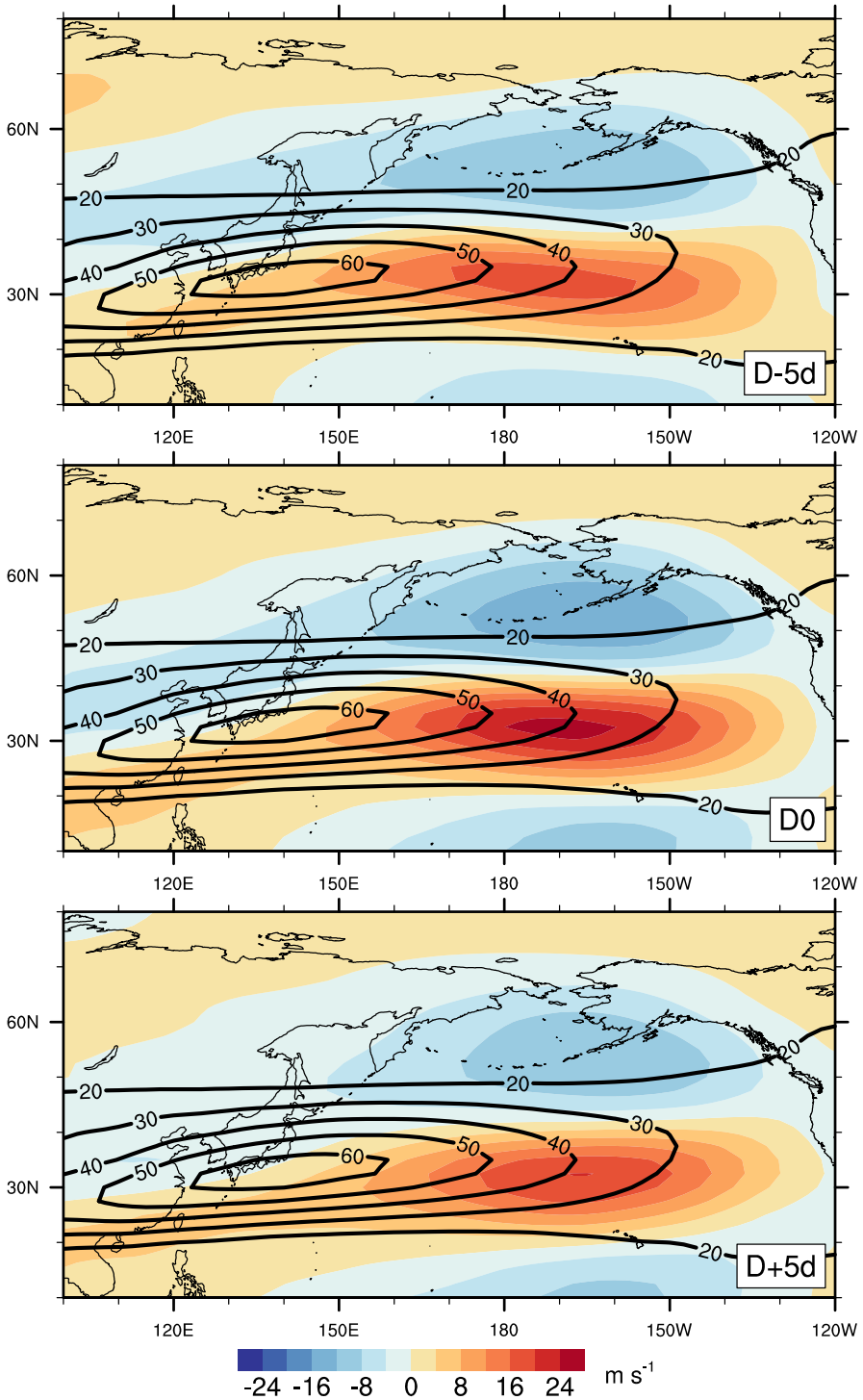

827

828 Fig. 2. TE-EOF 1 (extension/retraction) of the 250 hPa zonal wind over the North
829 Pacific. EOF regressed back onto anomaly data is shaded (m s^{-1}; per color bar).
830 Climatological zonal wind is contoured in black starting at 20 m s^{-1}. Top panel (D-
831 5d) represents the TE-EOF pattern at the beginning of the 10-day TE window;

middle panel (D0) represents the pattern halfway through the TE window; bottom panel (D+5d) represents the pattern at the end of the TE window.

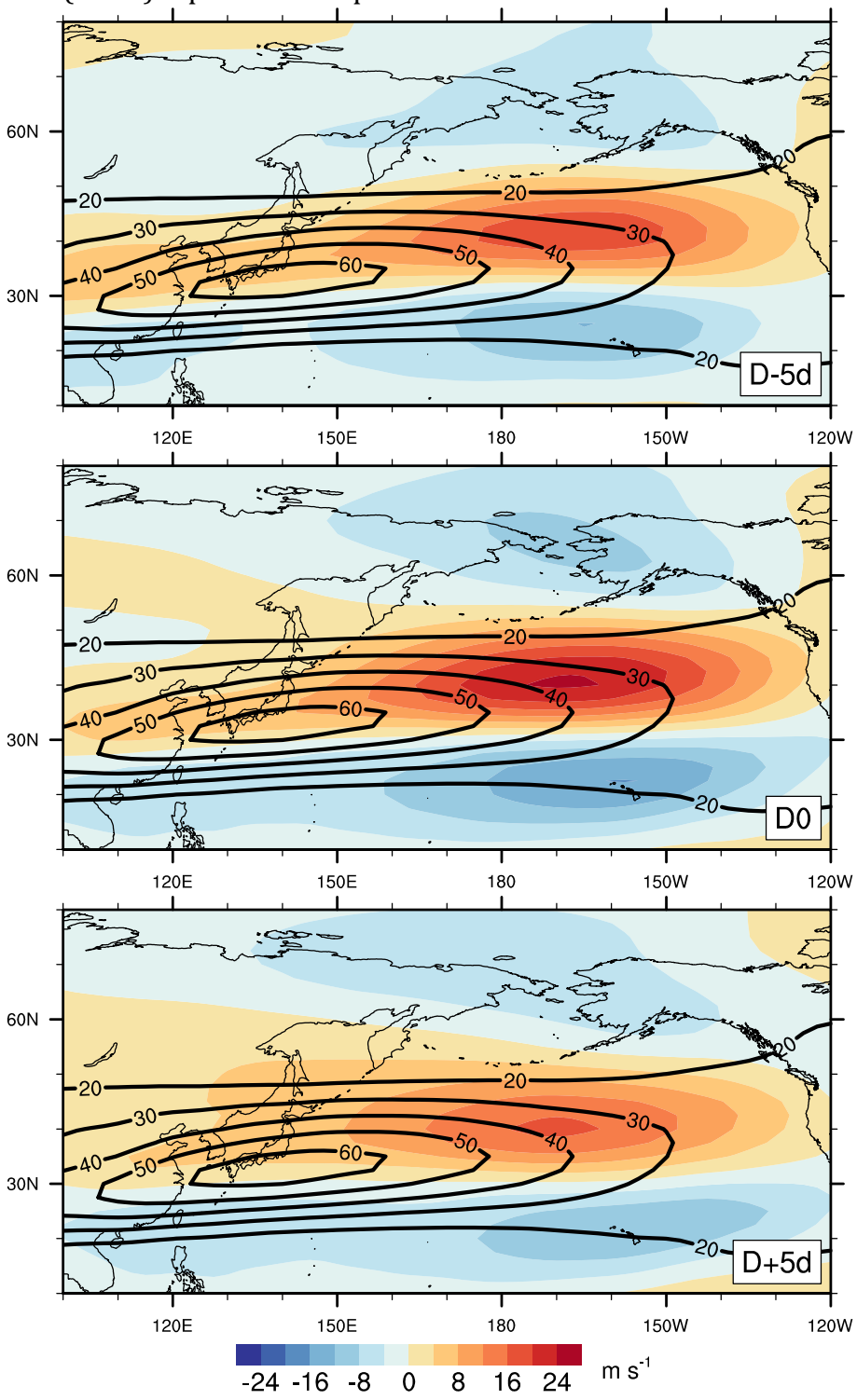

Fig. 3. As in Fig. 2 but for TE-EOF 2 (meridional shift) of the 250 hPa zonal wind over the North Pacific.

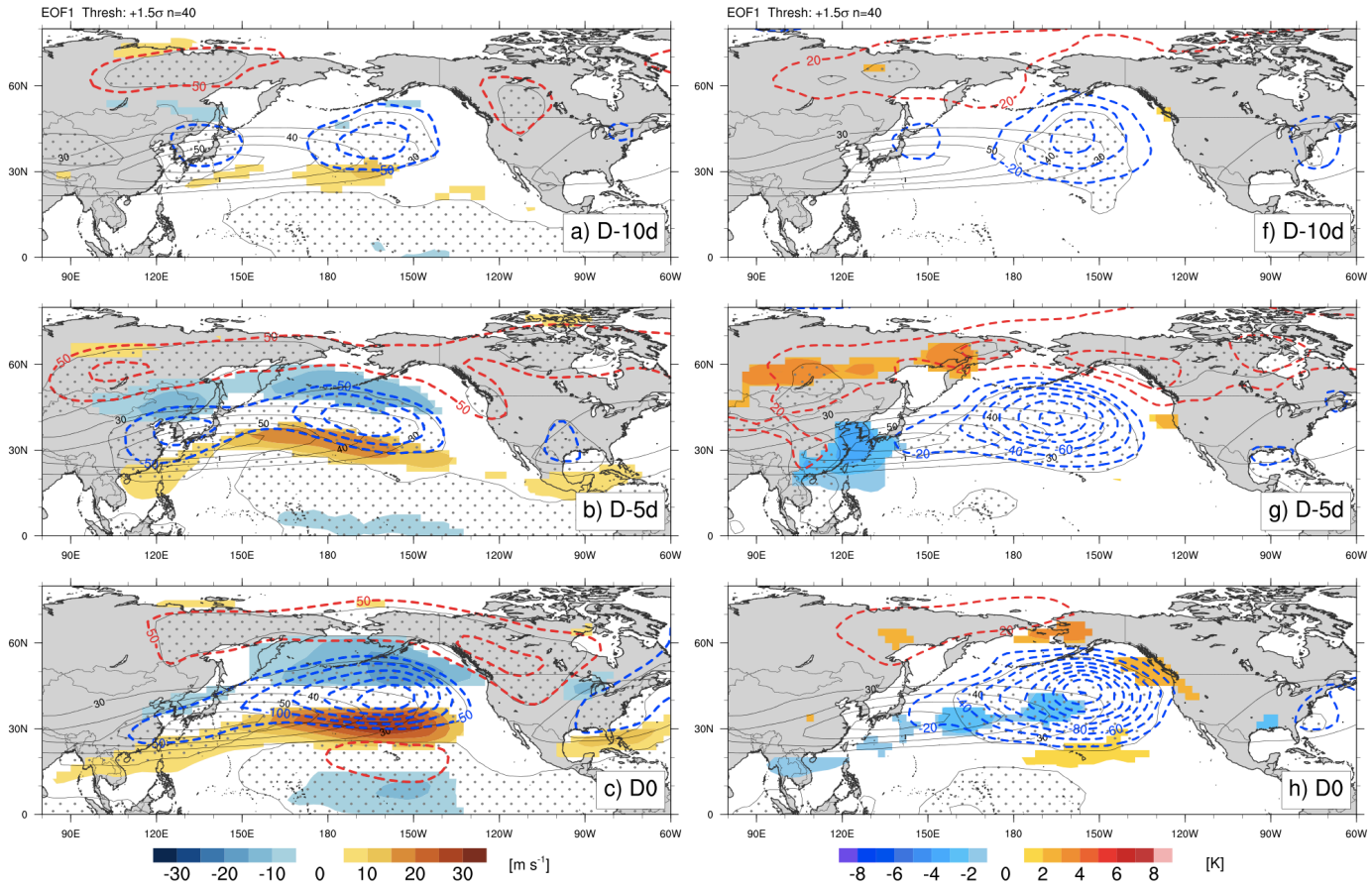

Fig. 4. Composite of cases where PC of TE-EOF 1 was positive and was greater than 1.5 standard deviations, representing jet extension cases. D0 is defined as the midpoint of the 10-day window, where D-5d (D+5d) is the beginning (end) point. Left plots (a-e) show anomalies of 250 hPa zonal wind (shaded per color bar; only where statistically significant at 95% level) and heights (dashed every 50 m). Right plots (f-j) include anomalies of 850 hPa temperature (shaded per color bar; only where statistically significant at 95% level) and heights (dashed every 20 m). Height anomalies in all plots are only significant within regional identified by stippling. All plots show the climatological zonal wind in thin black contours starting at 30 m s^{-1}. Composite sample size = 40.

845

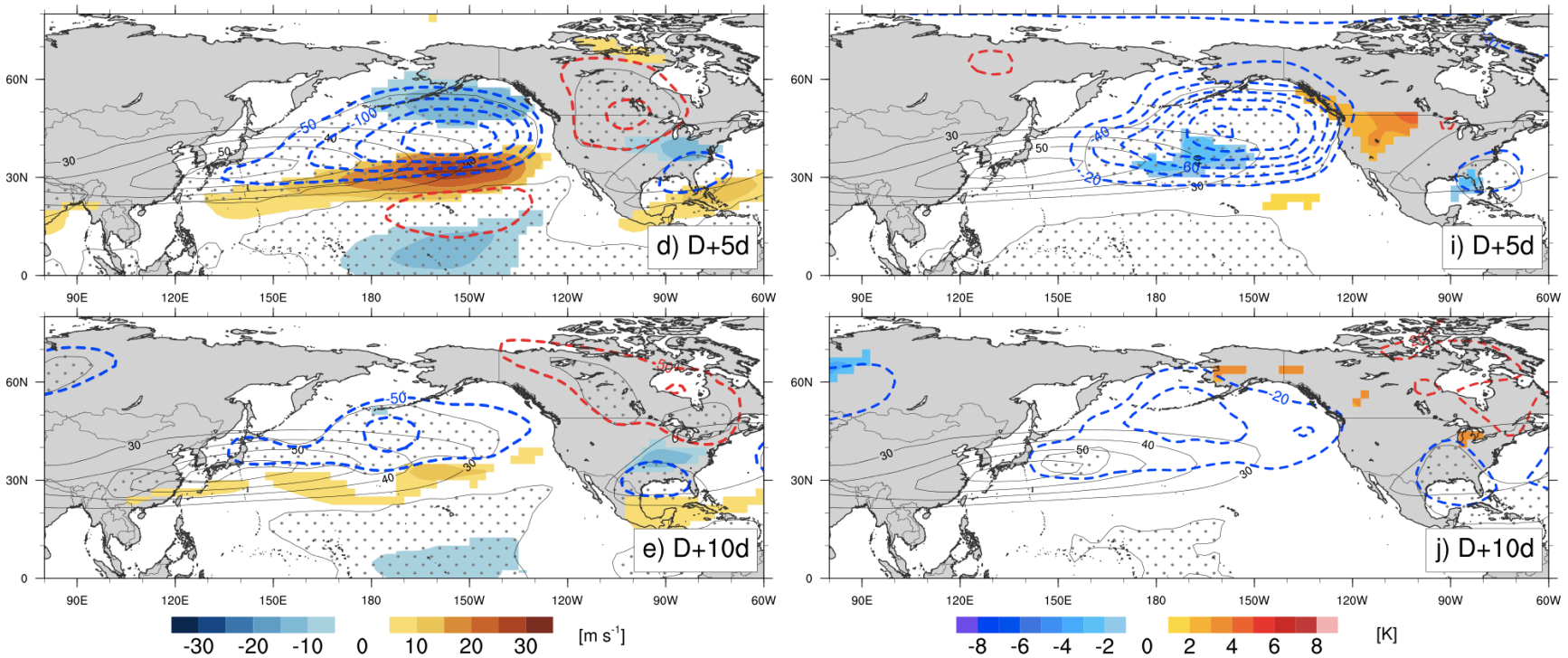

846

847 Fig. 4, continued.

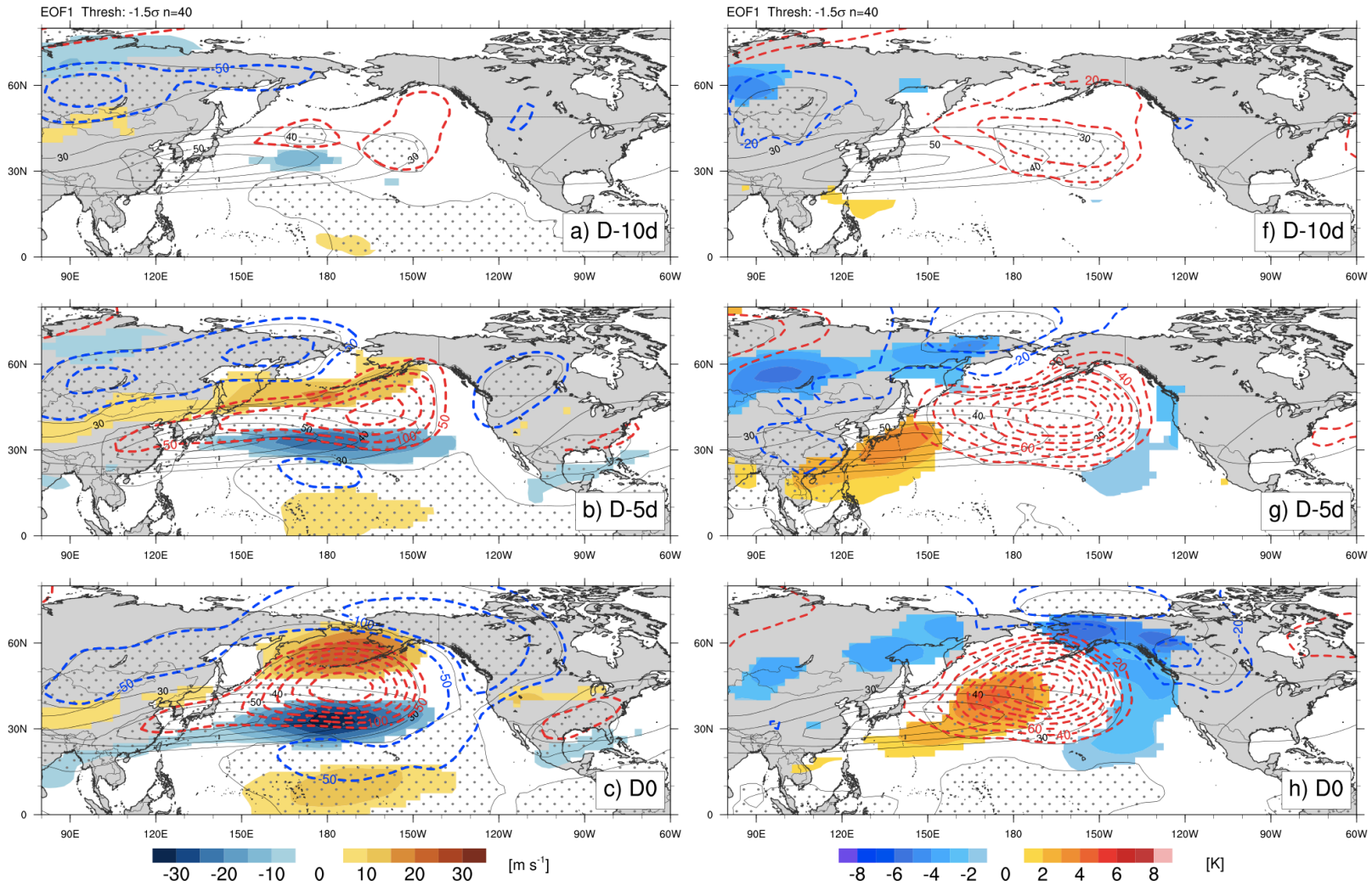

Fig. 5. As in Fig. 4 for cases where the PC of TE-EOF 1 was less than -1.5 standard deviations, representing jet retraction cases. Composite sample size = 40.

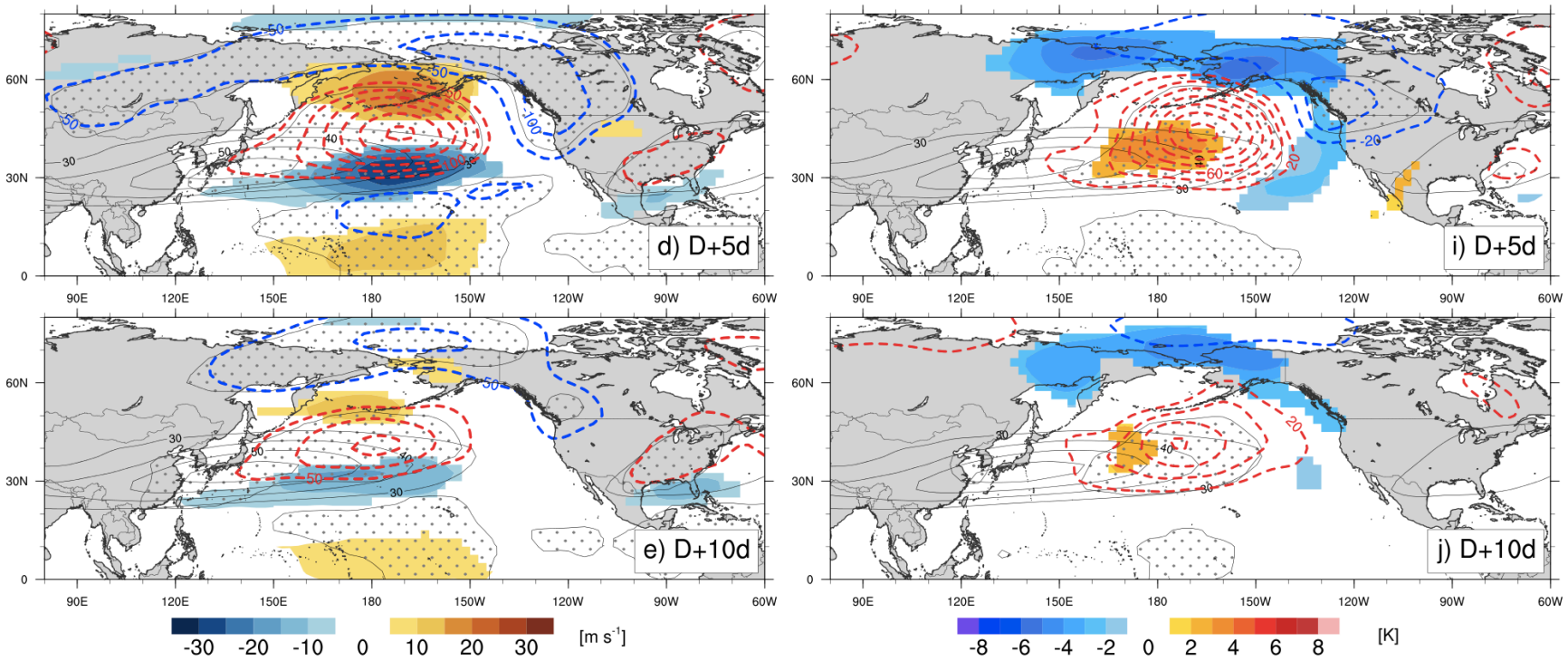

Fig. 5, continued.

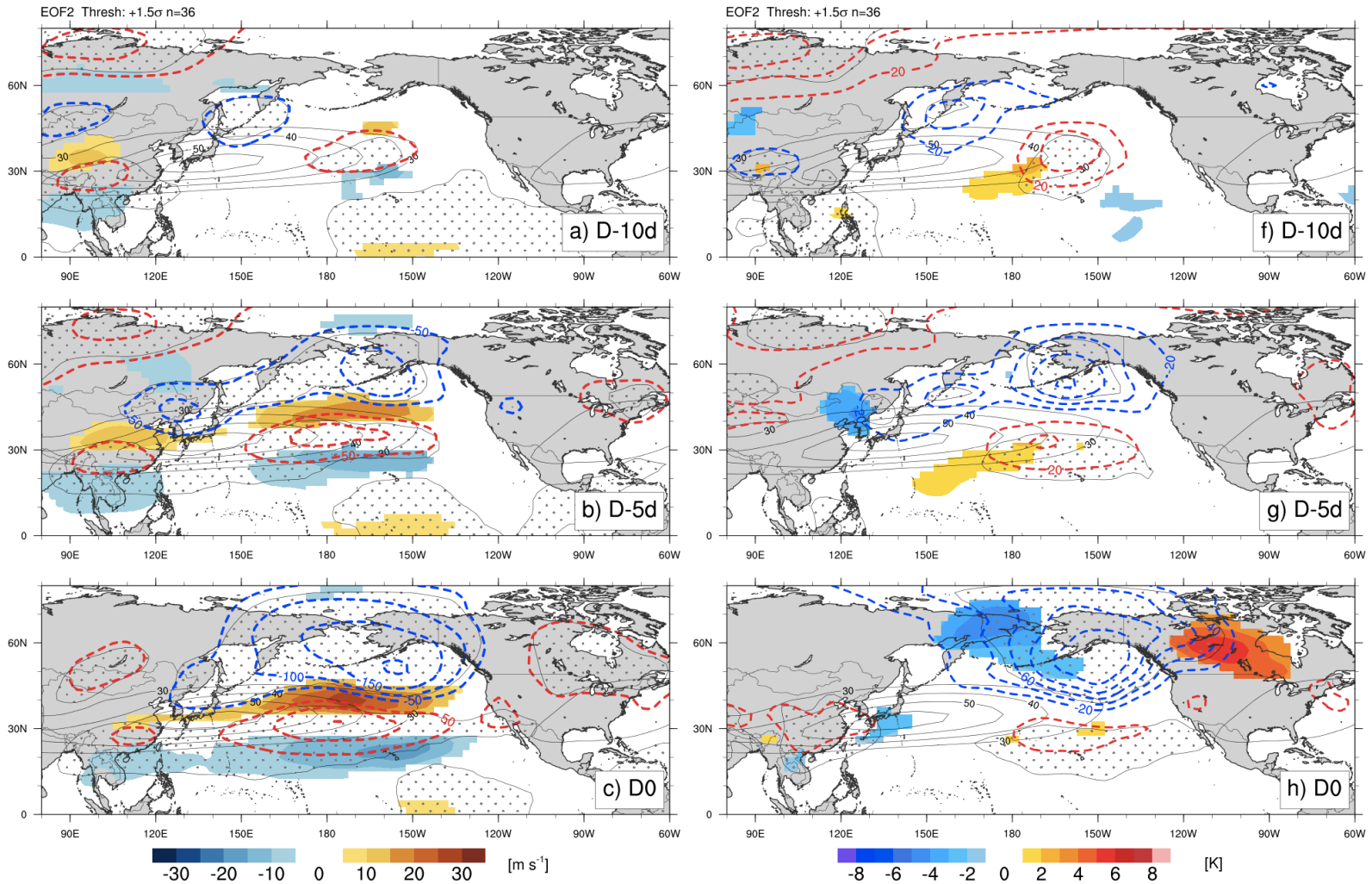

Fig. 6. As in Fig. 4 for cases where the PC of TE-EOF 2 was greater than 1.5 standard deviations, representing poleward shift cases. Composite sample size = 36.

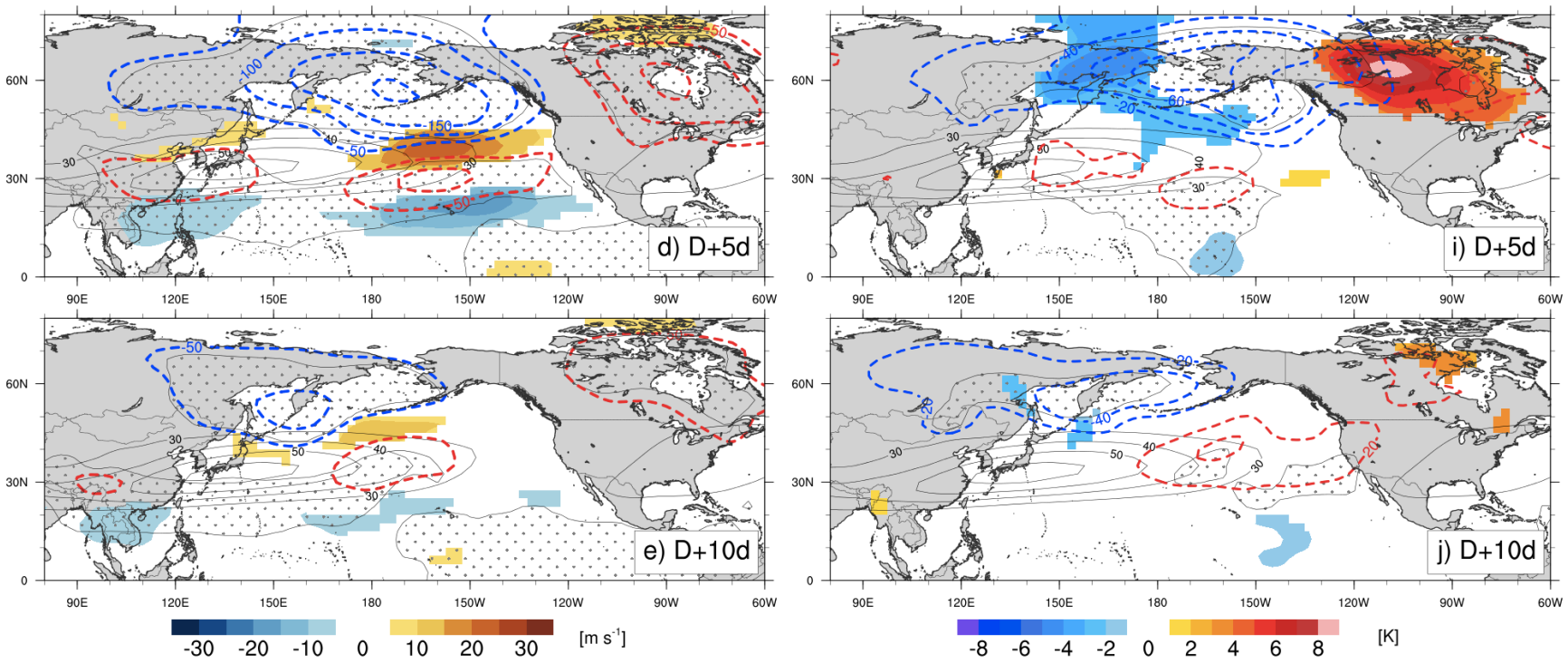

857
858 Fig. 6, continued.

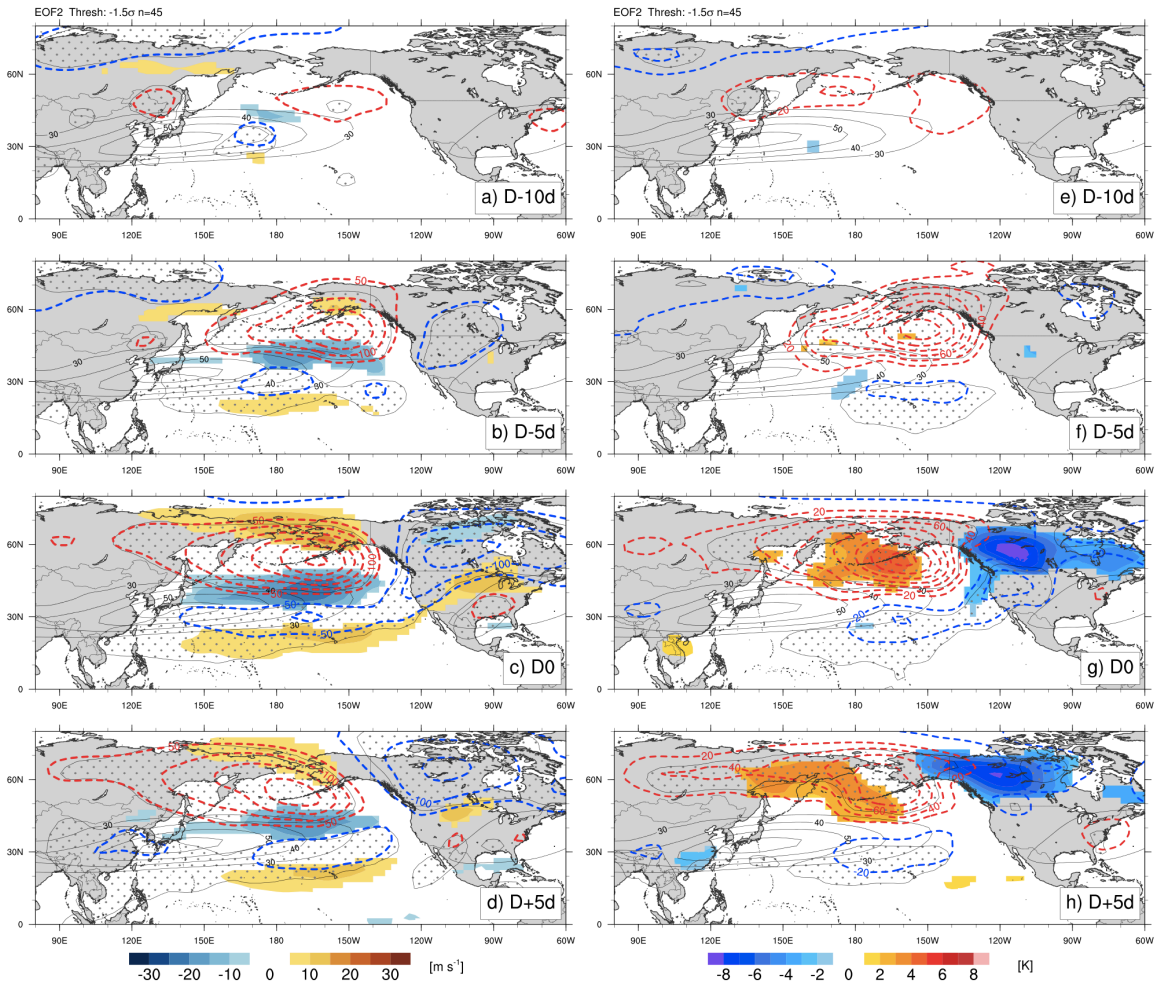

Fig. 7. As in Fig. 4 for cases where the PC of TE-EOF 2 was less than -1.5 standard deviations, representing equatorward shift cases. Composite sample size = 45. Unlike the previous composites, D+10d did not contain anomalies that appeared both physically meaningful and statistically significant.

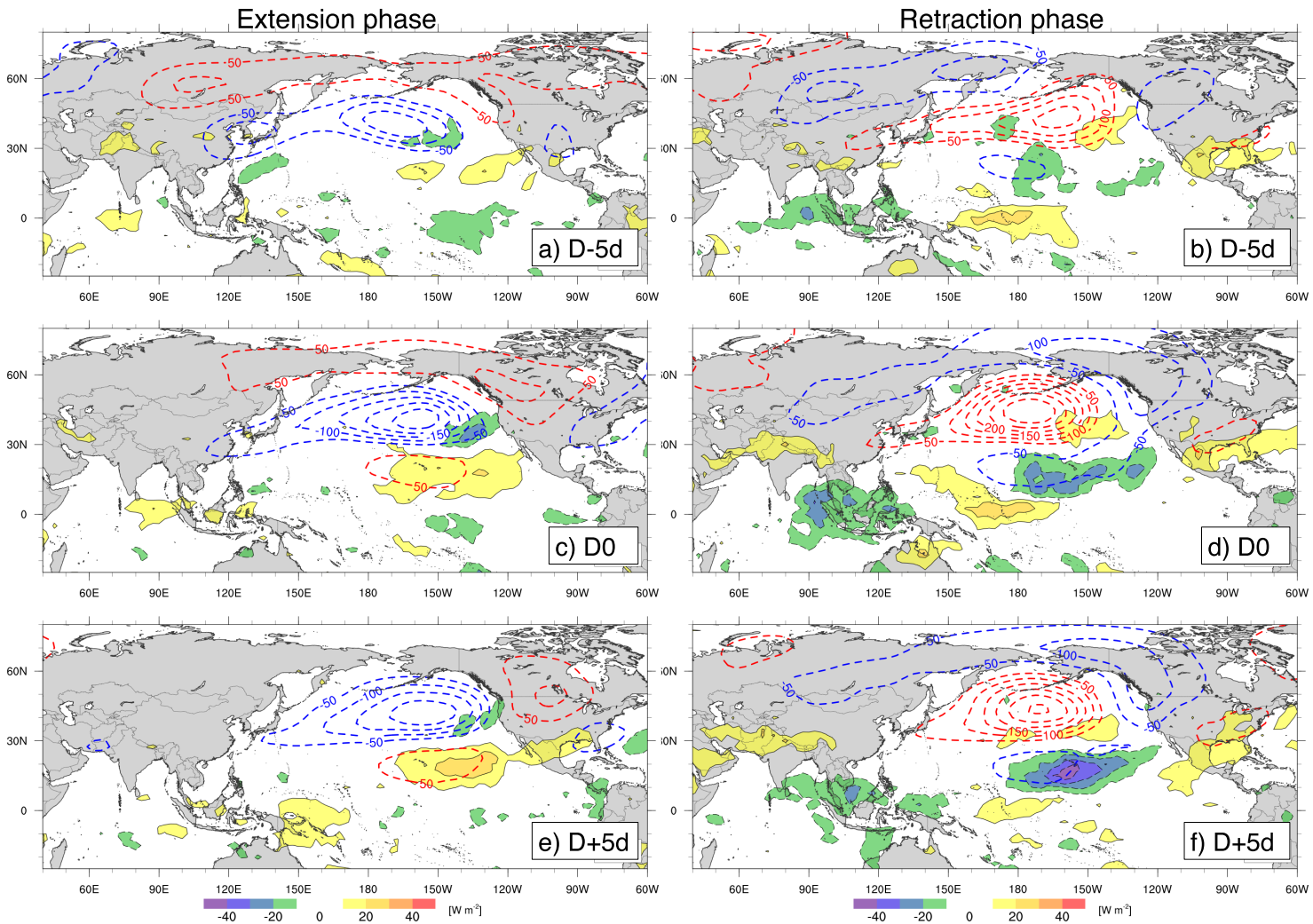

Fig. 8. Composites of OLR (shaded, per color bar) calculated as in Fig. 4 and Fig. 5 for jet extension (a, c, e) and jet retraction cases (b, d, f), respectively, from TE-EOF 1. Heights at 250 hPa contoured as in Fig. 4. Numbers of cases are consistent with the respective previous composites.

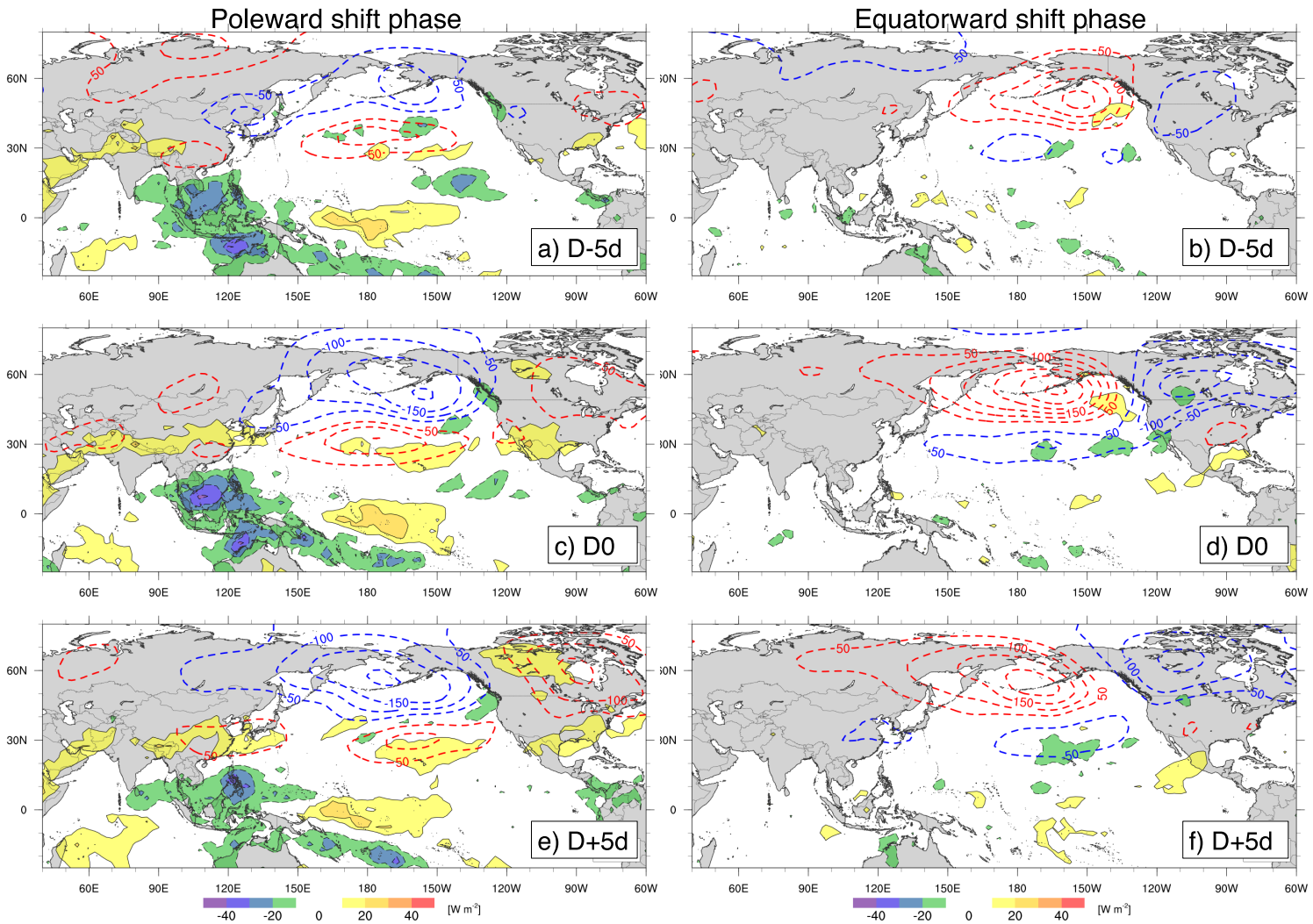

Fig. 9. As in Fig. 8 for poleward shift (from Fig. 6; a, c, e) and equatorward shift (Fig. 7; b, d, f) jet cases from TE-EOF 2. Heights at 250 hPa contoured as in Fig. 4. Numbers of cases are consistent with the respective previous composites.